materials

MDPI

Article

Control-Oriented Modeling of a 3D Printed Soft Actuator

Ali Zolfagharian [1,*], Akif Kaynak [1,*], Sui Yang Khoo [1], Jun Zhang [1], Saeid Nahavandi [2] and Abbas Kouzani [1,*]

[1] School of Engineering, Deakin University, Geelong, 3216, Australia; sui.khoo@deakin.edu.au (S.Y.K.); tzy@deakin.edu.au (J.Z.);
[2] Institute for Intelligent Systems Research and Innovation (IISRI), Deakin University; saeid.nahavandi@deakin.edu
* Correspondence: a.zolfagharian@deakin.edu.au (A.Z.); akaynak@deakin.edu.au (A.K.); abbas.kouzani@deakin.edu (A.K.)

Received: date; Accepted: date; Published: date

Abstract: A new type of soft actuator was developed by using hydrogel materials and 3D printing technology, attracting the attention of researchers, particularly in soft robotics field. Due to parametric uncertainties of such actuators, which originate in both custom design nature of 3D printing as well as time and voltage variant characteristics of polyelectrolyte actuators, a sophisticated model to estimate their behaviour is required. This paper presents a practical modeling approach for the deflection of a 3D printed soft actuator. The suggested model is composed of electrical and mechanical dynamic models that the earlier describes the actuator as a resistive-capacitive (RC) circuit, whereas the latter model relates the ionic charges to the bending of actuator. The experimental results were acquired to estimate the transfer function parameters of the developed model incorporating T-S fuzzy sets. The proposed model was successful in estimation of the end-point trajectory of the actuator especially in response to a broad range of input voltage variation. With some modifications in the electromechanical aspects of the model, the proposed modelling method can be used to other 3D printed soft actuators.

Keywords: Modeling; soft actuator; soft robot; 3D print

Introduction

In contrast to building robots from rigid materials in conventional robotics, soft, responsive, flexible and compliant materials have been used to make composite materials that can mimic biological systems. The study of such responsive composites is often referred to as soft robotics, which is a specific category of the field of robotics. There has been a growing interest in these materials which has potential applications in sensors and actuators. Functional components composed of soft and active materials can be 3D printed. Further, it was observed that monolithic structures independent of pneumatics or fluidics systems, which have their own shortcomings [1], can be developed as muscle like actuators by means of materials like shape memory alloys, shape memory polymers, or responsive hydrogel materials [1-3].

Using 3D bioprinting as part of fabrication of soft actuators from responsive materials such as hydrogel actuators with multi-material compositions with spatial control in interesting architectures has recently been investigated [4]. In a recent study polyelectrolyte chitosan hydrogel was used in the 3D printing of a soft actuator [5]. Chitosan has been found as an appropriate material for drug release, cell manipulation, and alike bio applications where the actuation and responsiveness to external stimuli is essential [6]. This has been mainly referred to its antibacterial properties which are attributed to free amino groups on the hydrogel backbone.

From one point of view hydrogels can be divided into two groups in terms of responsive behaviour to potential gradient. A group known as non-ionic hydrogels do not demonstrate a notable actuation response to input voltage when immersed in electrolyte solutions due to even distribution of hydrated ions on two sides of hydrogels. Polyelectrolyte hydrogels, however, react differently from non-ionic hydrogels when immersed into electrolyte solutions. Upon immersion in electrolyte solutions and applying voltages, polyelectrolyte hydrogels show actuation behaviour based on parameters like strength and polarity of input voltages and pH of solutions [7]. Various key factors, such as ionic charge and crosslinking densities as well as polymer and external electrolyte concentrations [7], have been identified to affect the amount of bending of polyelectrolyte hydrogels in response to an input voltage. For chitosan hydrogel when is immersed into an electrolyte solution with high pH, the carboxylic group would be deprotonated so as the hydrogel actuator take a negative charge. Then, upon the application of voltage potentials on electrodes, the hydrated cations enter to one side of the actuator more than other side. This result in an ionic strength difference between inside and outside of the hydrogel leading to a greater osmotic pressure on one side of hydrogel than the other side which in turn lead to bending of hydrogel actuator to the counter electrode or cathode. Thus, the gel near the anode swells, causing it to bend toward the cathode [8]. Noting that, along with osmotic pressure gradient, the ionic strength also affects the extent of bending of the polyelectrolyte soft actuator. While because of higher electric voltage the movements of ions are accelerated which lead to faster ionic and osmotic pressure gradients and therefore increase of both bending angle and bending rate of the actuator. Yet, the relation of bending behaviour of the actuator is not always proportional to ionic strength of electrolyte solution because of the shielding effect phenomenon [9].

Polyelectrolyte soft actuators have been considered as an electro-chemo-mechanical system that make their modeling quite complicated. The bending and actuation performances of polyelectrolyte soft actuators are influenced by uncertainties and time-varying parameters stemming from back relaxation and modulus variation phenomena. These undesirable factors should be dealt with for further fabrication and applications of such soft actuators. However, with incorporation of 3D printing in manufacturing of such soft actuators developing a control-oriented model for estimating the behaviour of these 3D printed polyelectrolyte soft actuators in real world application are demanded.

There have been studies on dynamics modelling of conventional polyelectrolyte soft actuators. Black-box models were used in some works for calculating the curvature of the actuator based on input voltage but were not scalable and too simple to describe the actuator performance entirely [10]. Advanced gray-box models based on electrical circuit models, like RC [11] and distributed transmission line models [12], have also been developed to correlate the applied voltage to the bending of the actuators [13]. More complex white-box models [10-12] considering complicated electro-chemo-mechanical principals have been developed to explain the more insightful details of underlying physics for accurate dynamics modeling of the polyelectrolyte actuators. Yet, these models realized too complex and not appropriate for real time control application of such actuators. This study establishes a mathematical gray-box relation of the 3D printed polyelectrolyte soft actuator by coupling both mechanical and electrical dynamics of the actuators.

Takagi-Sugeno (T-S) fuzzy modeling has been a practical approach in control designs applications [14], [15]. This study develops a reliable model of the 3D printed polyelectrolyte soft actuator based on the T-S fuzzy modeling strategy. The proposed model relates the different input voltages applied to the actuator to the bending of actuator via a universal T-S model surfing among the voltage dependent sub-models. This provides a scalable and practical model for further control applications of such systems.

The rest of paper is comprised of the following sections. First, 3D printing of the polyelectrolyte soft actuator using chitosan is explained. Then, an electro-chemo-mechanical modeling of 3D printed polyelectrolyte actuator is developed. Finally, the developed model is validated via the experimental tests data.

Fabrication of the Polyelectrolyte Actuator

Like other 3D print products, first, the actuator model was drawn in Solidworks (Dassault Systemes, USA) and then the model was imported into an EnvisionTEC GmbH Bioplotter software (EnvisionTEC, Gladbeck, Germany). The required materials including medium molecular weight chitosan (with *75–85%* deacetylation degree) and acetic acid solution were purchased from SigmaAldrich, Australia. A mixture of *1.6 g* chitosan in *0.8 ml* acetic acid solution (*1 v/v%*) was made under vigorous stirring at *50◦C*, for 2 h. The resultant 3D print ink was then prepared through sonication and centrifugation. Finally, the ready to print ink was poured into a low-temperature 3D Bioplotter syringe. For solidifying each layer after extrusion, a solution of Ethanolic Sodium Hydroxide (EtOH-NaOH) with *0.25 M* NaOH (Sigma Aldrich), *70 v/v%* EtOH (*3:7* ratio), was prepared. The porous chitosan beam with the size of *40 mm* by *8 mm* by *2 mm* was printed layer by layer (Fig. 1(a)). The 3D printing was performed with optimized parameters of 3D Bioplotter as explained extensively in an earlier work of authors [16].

Electro-Chemo-Mechanical Model of the 3D Printed Polyelectrolyte Actuator

To circumvent the complexity of Multiphysics modeling, this study suggests a scalable model of the polyelectrolyte actuator. Doing so, various factors are considered in the behavior of the actuators to estimate the dynamics parameters more realistically. Thus, the actuator model comprises both electrochemical and electromechanical models considering their dynamics coupling.

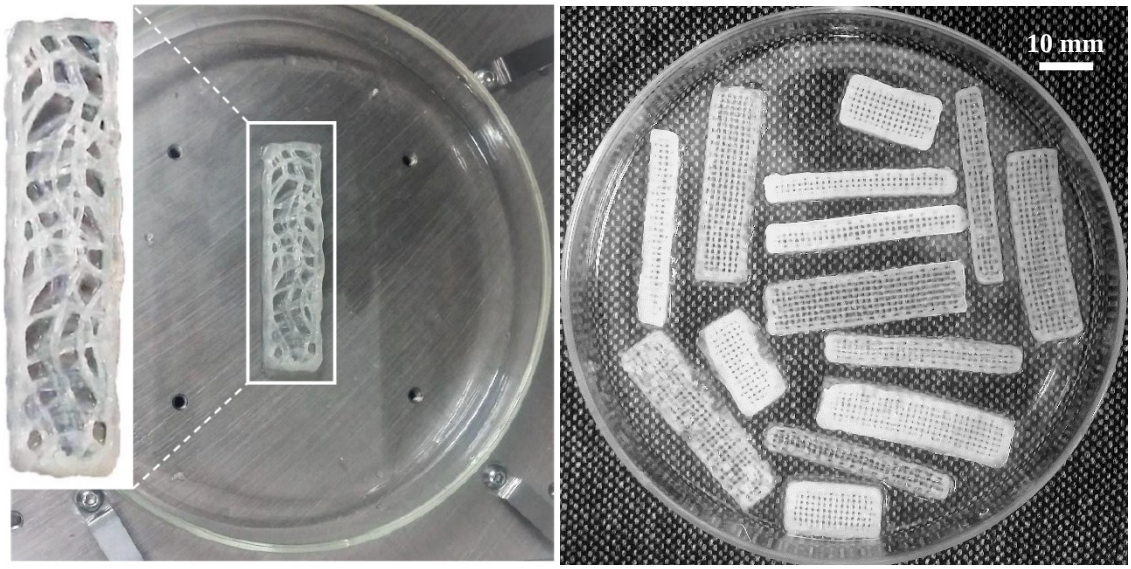

(a) (b)

Figure 1. (a) An arbitrary pattern 3D printed polyelectrolyte actuator; (b) different patterns and sizes of 3D printed polyelectrolyte actuators.

Electrochemical Modelling

An electrochemical RC model that gives the relation between applied voltage and current flown across the polyelectrolyte gel is illustrated in Fig. 2. A diffusion model to represent the current flow across the 3D printed polyelectrolyte actuator are calculated from the Fick's law of diffusion as:

$$i_D(t) = -F \times A \times D \times \frac{\partial c(y,t)}{\partial y}, \quad (1)$$

where (c) refers to the ion concentration, the path along the thickness of the actuator is indicated by y, (D) is the diffusion coefficient constant, (A) is the area between the interface of electrolyte solution and polyelectrolyte actuator, and (F) denotes the Faraday constant. Then, the current running across the double layer capacitance can be calculated assuming the double-layer capacitance thickness as (δ):

$$i_C(t) = F \times A \times \delta \times \frac{\partial c(y,t)}{\partial y}. \quad (2)$$

Next, for a 3D printed polyelectrolyte actuator with the thickness of the (h), the diffusion equation model can be written as:

$$\frac{\partial c(y,t)}{\partial t} = D\frac{\partial^2 c(y,t)}{\partial y^2} \quad 0 < y < h, \ \frac{\partial c(y,t)}{\partial t}(@y = h) = 0. \quad (3)$$

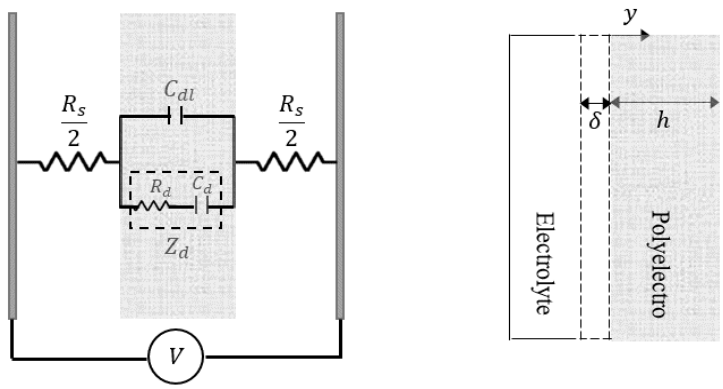

Figure 2. Equivalent RC circuit where (Z_d) is the diffusion impedance, (C_{dl}) denotes the double layer capacitance, and (R_s) refers to the resistance the electrolyte solution.

Finally, an electrochemical model relating the current flown across the actuator to the applied voltage can be obtained by simultaneous solving the Eqs. 1-3 as:

$$\frac{I(s)}{V(s)} = \frac{s\left[\frac{\sqrt{D}}{\delta}\tanh\left(h\sqrt{\frac{s}{D}}\right)+\sqrt{s}\right]}{\frac{\sqrt{s}}{C_{dl}}+s\sqrt{s}R_s+R_s\frac{\sqrt{D}}{\delta}s\tanh\left(h\sqrt{\frac{s}{D}}\right)}. \quad (4)$$

Electromechanical Modelling

An electromechanical model that relates the osmotic pressure caused by input voltage to the bending of 3D printed polyelectrolyte actuator is developed in this section. Assuming the strain-to-charge ratio α, the relation between the charges density (ρ_{ch}) and resulted in-plane strain (ε) in polyelectrolyte actuators can be written as [18]:

$$\varepsilon = \alpha\rho_{ch}\,, \quad (5)$$

where for a 3D printed soft actuator with size of (W) and (L) as width and length respectively, (ρ_{ch}) can be calculated as:

$$\rho_{ch} = \frac{1}{WLh}\int_0^t I(t)dt \xrightarrow{L} \rho_{ch}(s) = \frac{I(s)}{sWLh}, \quad (6)$$

Generally, actuators strains are calculated knowing the tip displacement, initial length and thickness of the actuators when the bending curvature is comparatively small. But, the curvature radius is not negligible when the soft actuators experience larger bending. In this study, as shown in Fig. 3 and Eq. 7, the strain (ε) resulted purely from bending of the actuator is obtained as:

$$\varepsilon = \frac{l_o - l_c}{l_c} = \frac{(R+y)\theta - R\theta}{R\theta} = \frac{y_b}{R} = Ky_b\,, \quad (7)$$

where (l_o) and (l_c) are the swelled length and the centered length of actuators, (θ) and (R) refer to the bending angle and the radius of curvature of the actuator respectively, (y_b) shows the distance between the outer edge of swelled layer and the reference plane, and (K) is the bending curvature of the actuator. To estimate an accurate value of the stress induced on the bending of actuator the superposition of actuations effect and the bending strain are considered together, so, the total induced

stress, assuming the Young's modulus of the 3D printed polyelectrolyte actuator as (E), can be calculated as follows:

$$\sigma = E(K \mp \alpha\rho_{ch}), \tag{8}$$

where the opposite signs representing the expansion and contraction of sides of actuators.

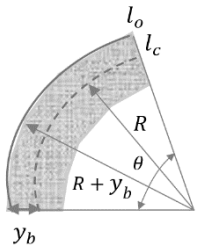

Figure 3. Schematic of the bending of the printed actuator.

Equaling the total moments and forces on the actuators to zero, the bending curvature (K) can be realized. This is somehow related to a new defined coefficient φ as follows:

$$\sum F = \int_{-h/2}^{0} E(Ky_b + \alpha\rho_{ch})y_b dy_b + \int_{0}^{h/2} E(Ky_b - \alpha\rho_{ch})y_b dy_b = 0,$$

$$\sum \sigma = \int_{-h/2}^{0} E(Ky_b + \alpha\rho_{ch})dy_b + \int_{0}^{h/2} E(Ky_b - \alpha\rho_{ch})dy_b = 0, \tag{9}$$

$$K = \varphi\rho_{ch}, where\ \varphi = \frac{3\alpha}{Eh}.$$

Combining Eqs. 9 and 6 into Eq. 4, bending curvature can be expressed as:

$$K(s) = \frac{\varphi V(s)}{WLh} \frac{\left[\frac{\sqrt{D}}{\delta}\tanh\left(h\sqrt{\frac{s}{D}}\right) + \sqrt{s}\right]}{\frac{\sqrt{s}}{C_{dl}} + R_s s\sqrt{s} + R_s \frac{\sqrt{D}}{\delta} s \tanh\left(h\sqrt{\frac{s}{D}}\right)}. \tag{10}$$

Finally, the model relating the applied voltage to bending of the 3D printed polyelectrolyte actuator can be obtained by incorporating Eq. 6 and Eqs. 5-10 as following [19]:

$$\frac{Y(s)}{V(s)} = \frac{\varphi}{WLh} \frac{1}{sR_s + \frac{1}{C_{dl}\left[1 + \frac{\sqrt{D}}{\delta\sqrt{s}}\tanh\left(h\sqrt{\frac{s}{D}}\right)\right]}}, \text{ where, } Y(s) = \frac{1}{K(s)} \mp \sqrt{\frac{1}{K(s)^2} - L^2}. \tag{11}$$

The Eq. 11 needs to be restructured to be practical for control applications due to presence of hyperbolic tangent term in its denominator leading to be dimensionally infinite. To deal with this, the dimensionally infinite hyperbolic tangent term can be replaced by Mittag Leffler's expansion as:

$$\frac{\tanh(\frac{1}{2}\sqrt{\frac{X}{Y}})}{4\sqrt{XY}} = \sum_{n=0}^{\infty} \frac{1}{X + n^2((2n+1)^2 Y)}, \tag{12}$$

where $X = s$, and $Y = D/4h^2$. This simplification confines the model in a bounded range of frequencies for input voltages within the interest low frequency range for the 3D printed polyelectrolyte soft actuator. Hence, Eq. 12 represents the model for the small values of (n), so as a fourth order model approximates bending displacement of the 3D printed soft actuator as:

$$\frac{Y(s)}{V(s)} = e^{\beta s} \frac{(s + z_1)(s + z_2)(s + z_3)}{(s + p_1)(s + p_2)(s + p_3)(s + p_4)}, \tag{13}$$

where β is a real value and z_i's (n=1,2,3) are the zeros and p_i's (n=1,2,3,4) are the poles of the soft actuator transfer function.

T-S Fuzzy System Modeling Formulation

Consider a simplified dynamic system without uncertainties systems as:

$$\dot{x} = A(x) + B(x)u. \tag{14}$$

Fuzzy inference rules for T-S fuzzy dynamic model of Eq. 16 can be described as follows [20]:

R^i: $IF\ z_1 is\ w_1^i\ AND \dots\ z_n\ is\ w_n^i$

$THEN$

$$\dot{x} = A^i(x) + B^i(x)u \ \text{ for } \ i = 1, \dots, m, \tag{15}$$

where the matrices $A^i \in R^{n\times n}$ and $B^i \in R^{n\times 1}$ represents the subsystem parameters, $z = (z_1, \dots, z_n)^T$, behavior. x is system state variable vector and u is the system input. R^i represents the ith fuzzy inference rule, $z(t) = [z_1(t)\ z_2(t) \dots\ z_n(t)]$ among m number of inference rules.
Knowing $M_j (j = 1, \dots, n)$ are the fuzzy sets, the inferred fuzzy set w^i can be used to calculate μ_i as the normalized fuzzy membership function of inferred fuzzy sets as follows:

$$w^i = \prod_{j=1}^{n} M_j^i, \qquad \mu^i = \frac{w^i}{\sum_{i=1}^{m} w^i}, and \sum_{i=1}^{m} \mu^i = 1. \tag{16}$$

The singleton fuzzifier, product inference, and center-average defuzzifier are used to form the global dynamic fuzzy model of the nominal system of Eq. 17 as:

$$\begin{gathered} \dot{x} = A(\mu)x + B(\mu)u(t)\,, \\ A(\mu) = \sum_{i=1}^{m} \mu^i A^i, B(\mu) = \sum_{i=1}^{m} \mu^i B^i, where\ \mu = (\mu^1, \mu^2, \dots, \mu^m)\,. \end{gathered} \tag{17}$$

Actuator Characterization

The bending of the 3D printed polyelectrolyte hydrogel actuator can be justified by Donnan effect phenomenon. This means that the motion of counterions initiated by applied voltage leads to the ionic gradient within the hydrogel networks along the direction of the electric field. This results in an osmotic pressure difference within the hydrogel structure, and consequently causes the deflection of 3D printed actuator toward the counter electrode. Several factors can be considered to characterize the behaviour of the actuator. First, the effects of the electrolyte solution and its concentration on the bending behaviour of the 3D printed polyelectrolyte actuator should be defined. Doing so, two different electrolyte solutions, NaOH and NaCl, were opted to test the 3D printed actuator endpoint deflection behaviour. The maximum endpoint deflection for the same sizes (40mm × 8mm × 2mm) and patterns of 3D printed actuators are measured with respect to the ionic strength of the electrolyte solutions. A constant voltage of 5 V was applied between the electrodes and the concentration of NaOH and NaCl solutions were set in the range of [0.1, 0.2] M with increment of 0.2 M for each experiment. The experiments repeated three times and results are depicted in Fig. 4(a). Regardless of concentration of electrolyte solution, actuator has reached to more deflection in NaOH solution than in NaCl solution. Also, it is observed that for both electrolyte solution there were an optimum value for electrolyte ionic strength to achieve maximum bending angle. As shown in Fig. 4, this optimum value for the 3D printed actuator tested here was nearby 0.12 M. It is seen that from 0.1 to 0.12 M the endpoint deflection of the 3D printed actuator increased. This can be attributed to an increase of the free ions moving from the surrounding solution toward their counter-electrodes. However, if the concentration of the solutions were greater than the critical concentration, 0.12 M, the shielding effect of the poly-ions occurred leading to a reduction in the electrostatic repulsion of the poly-ions, and the subsequent decrease in the endpoint deflection. Hence, in the rest of paper all tests are performed in NaOH electrolyte solution of 0.12 M.

Furthermore, several different patterns and dimensions of the actuators with the same material are 3D printed (Fig. 1(b)). Then, the behaviour of the 3D printed actuators based on different dimensions are investigated and the results are inserted in Table 1. The results reveal that the

maximum endpoint deflection of the actuators increase in proportion to their length while it shows almost no correlation with the width of the actuator. It was also observed that the bending deflection was inversely correlated to the thickness of the actuator [4].

To reveal hysteresis behaviour of 3D printed actuator the repeatability tests were performed. The same pattern and size of 3D printed samples of actuators were excited with a square wave electrical stimulus. The magnitudes of the square waves were selected as 5 V with the period of 220 s and duty cycle of 50%. The duration of experiment was set to be 5 times of period, and the performances of the actuators were compared based on change in maximum magnitudes in each cycle as shown in Fig. 4(b). The results showed that all actuators reached their maximum deflections at the first set of experiments for a specific excitation voltage.

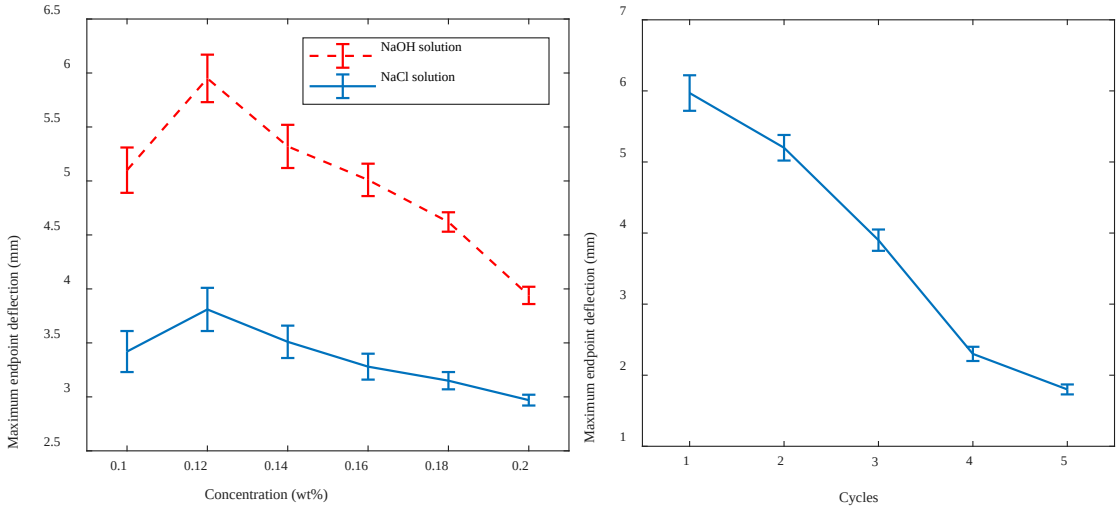

Figure 4. (a) Response of the actuators with same pattern and dimensions to different electrolyte solutions; (b) maximum endpoint deflections of the actuators to 5 V input signal over different cycles. Error bars indicate the standard deviation of the maximum distance measured over the three trials.

Table 1. Results of maximum endpoint deflection for same pattern and different sizes of 3D printed actuators.

Actuator	Length (mm)	Width (mm)	Thickness (mm)	Maximum deflection (mm)
S1	40	8	2	5.92
S2	40	8	1	8.27
S3	40	4	2	5.38
S4	20	8	2	1.83

In next stage, actuator's endpoint deflections were tested overtime based on different input voltage magnitudes as illustrated in Fig. 5. From the results, it can be deduced that the actuation performance increased in the higher voltage; however, the occurrence of electrolyses and bubbling in electrolyte caused undesirable effects and limit application of higher voltages in such actuators.

Actuator responses under various frequencies were also investigated. Square voltage of 5V was applied between two electrodes in various frequencies, 0.0025, 0.02, 0.031, 0.054, 0.11, 0.15, and 1.1 Hz. It can be seen from figures 6(a) that the maximum endpoint deflections decrease with increasing frequency since the actuators have less time to respond. Also, response time to the first peak were measured and were demonstrated in figure 6(b). From the figure can be observed that the actuator reaches the first peak faster as the magnitude of the peaks decrease in higher frequencies.

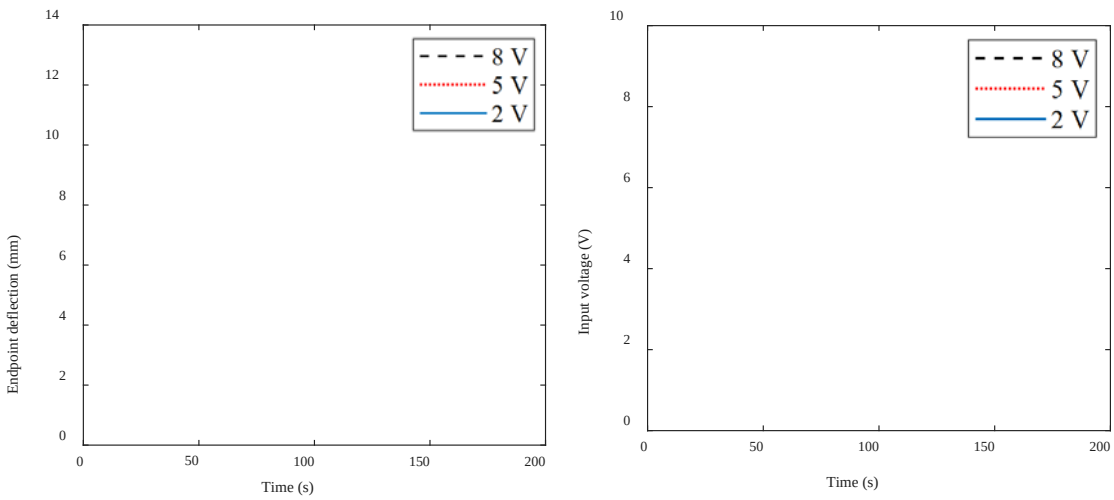

(a) (b)

Figure 5. (a) Response of the actuators with same pattern and dimensions to (b) different input voltages' magnitudes. The results are averaged over the three trials.

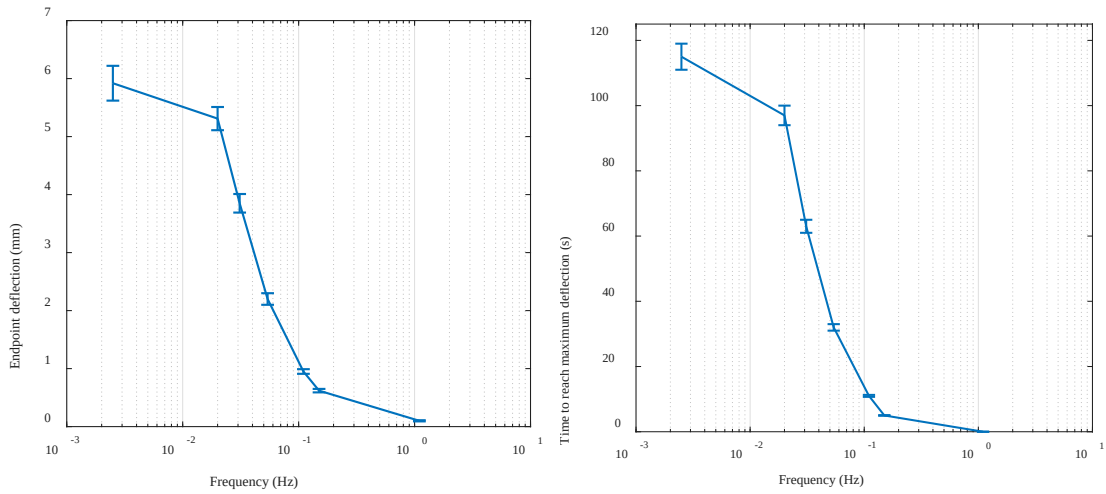

(a) (b)

Figure 6. (a) Response of actuator's maximum endpoint deflection to various frequencies under 5 V square waves; (b) response time to first peak. Error bars indicate the standard deviation of the maximum distance measured over the three trials.

Modelling and Experimental Results

Now Golubev method [21] is used to estimate an appropriate model for control of actuator [22-25]. Using Golubev method for the input signal, the uncertain transfer function relating the applied voltage to the bending angle of the actuator is estimated as:

$$G(s) = e^{\beta s}\frac{a_1 s^3 + a_2 s^2 + a_3 s + a_4}{b_1 s^4 + b_2 s^3 + b_3 s^2 + b_4 s + b_5}, \tag{18}$$

The frequency response model of the actuators with different patterns and sizes, shown in Fig. 1(b), are identified based on Eq. (18) and the experimental data are depicted in Fig. 7. It is observed that changing various parameters of the actuator, like different sizes and patterns, lead to a new set of linear voltage dependent transfer functions. Therefore, for each specific actuator a system identification of frequency response to different voltage levels are required. Then, T-S fuzzy model should be incorporated to interrelate the linear transfer functions at different voltage levels for improving the model accuracy.

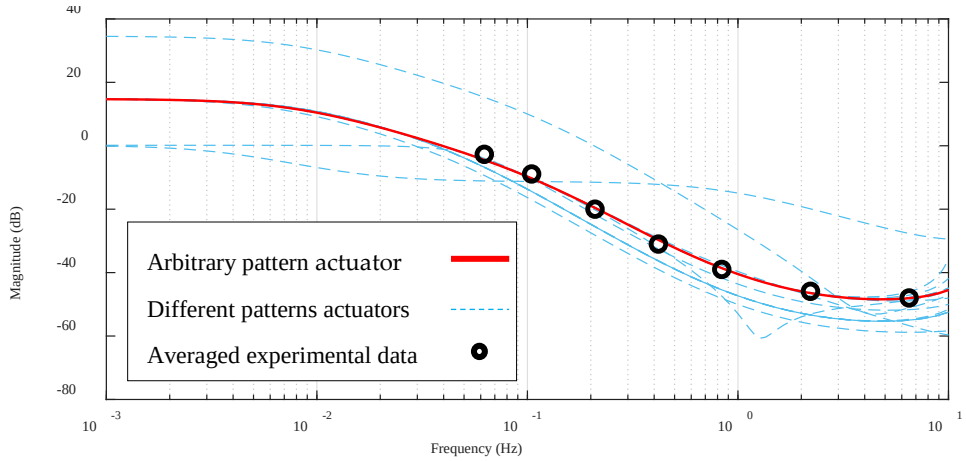

Figure 7. Frequency response system identification of different 3D printed actuators in response to 5V input signal.

To identify transfer function parameters for the arbitrary pattern actuator S1, lower and upper limit input signals, 2V (shown in Fig. 8a) and 8V are applied to the system and the range of parameters identified as follows:

$a_1 \in [0.0063,0.0085]$; $a_2 \in [0.6381,0.842]$; $a_3 \in [1.152,1.924]$; $a_4 \in [1.14,1.97]$;
$b_1 \in [1,1]$; $b_2 \in [0.3631,0.5898]$; $b_3 \in [225.5,367.2]$; $b_4 \in [14.98,29.41]$; $b_5 \in [0.2142,0.2275]$;
$\beta = -3.67$.

Then, a two-rule based T-S model is defined as:

Rule 1: IF $|z(t)| \leq 5$ THEN $\dot{x} = A_1 x(t) + B_1 u(t)$.

Rule 2: IF $5 < |z(t)| \leq 8$ THEN $\dot{x} = A_2 x(t) + B_2 u(t)$.

Finally, the outputs of the T-S fuzzy model (shown in Fig. 7b) can be calculated as:

$$\dot{x} = \mu_1\big(z(t)\big)\big(A_1 x(t) + B_1 u(t)\big) + \mu_2\big(z(t)\big)\big(A_2 x(t) + B_2 u(t)\big), \quad \text{where } \mu_1\big(z(t)\big) + \mu_2\big(z(t)\big) = 1. \tag{19}$$

A comparison of experimental tests with the T–S fuzzy model and estimated specific voltage models for 2V and 8V input signals is shown in Figs. 9 and 10. The data is the average of three experiments to confirm reproducibility. Also, the efficacy of the developed model in terms of scalability of the 3D printed soft actuators with different patterns and sizes are shown in Figs. 10(b) and 10(c) where two actuators with arbitrary and lattice patterns and sizes S1 and S4 are compared in response to an analogous input. These figures show supremacy of actuator end-point position estimation by T-S fuzzy modelling compared to specific constant voltage models even with changing the 3D printed actuator parameters such as pattern and size. Furthermore, looking at Fig. 10(b) in detail reveals some discrepancy of the T-S model from experimental results, especially over longer experimental tests. This is attributed to the time-varying intrinsic nature of the polyelectrolyte soft actuator that demands feedback controller for compensation purpose in future study.

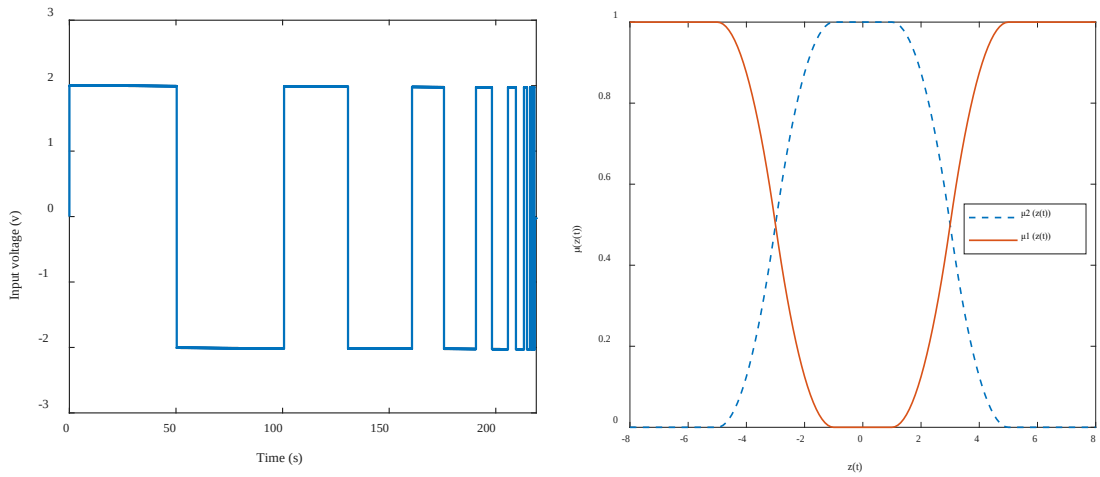

(a) (b)

Figure 8. (a) An example of input signal for model identification (2v); (b) membership function of T-S model.

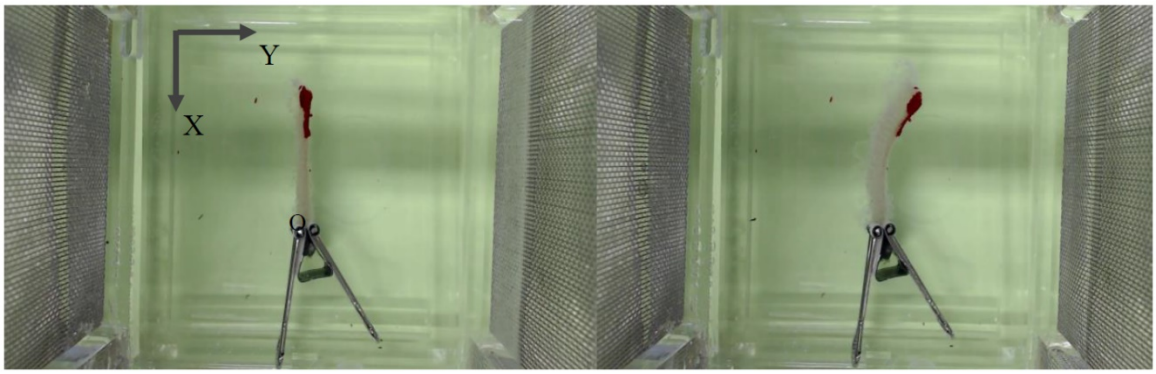

Figure 9. Bending of the printed actuator under applied voltage.

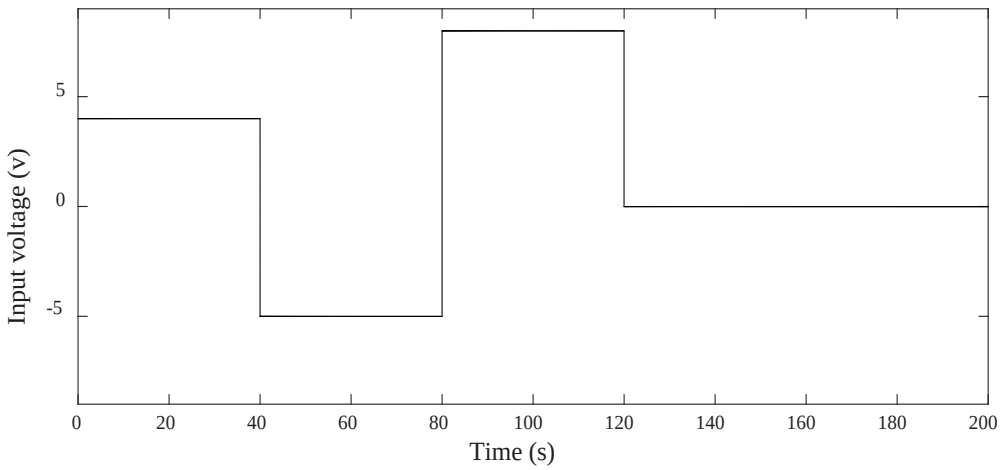

(a)

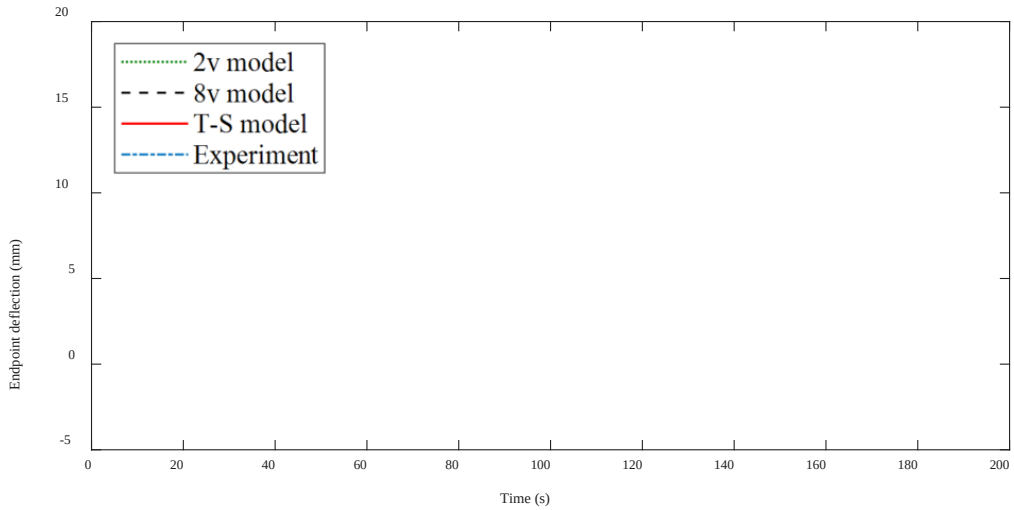

(b)

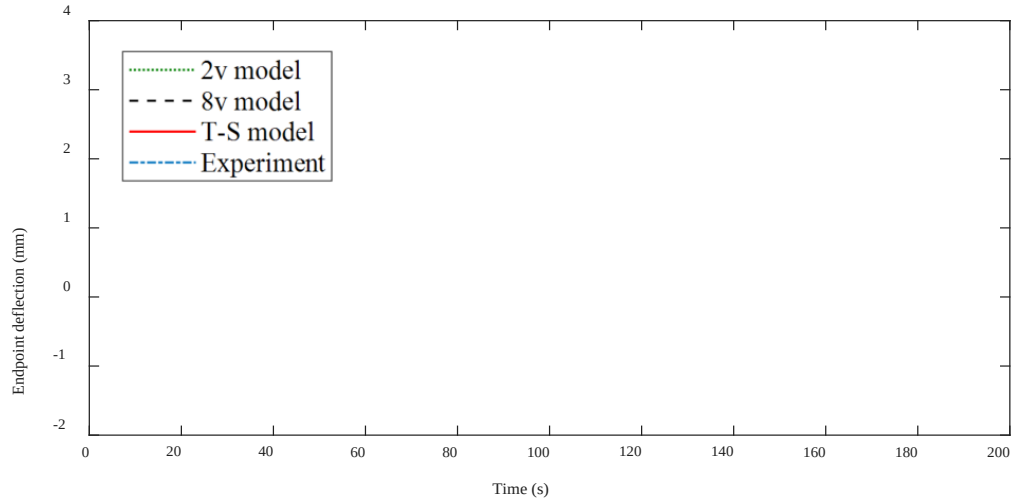

(c)

Figure 10. (a) Input voltage signal; (b) endpoint deflection of arbitrary pattern actuator with size of S1; (b) endpoint deflection of lattice pattern actuator with size of S4.

Conclusion

A control-oriented modelling approach for 3D printed polyelectrolyte soft actuators was presented in this study. First, 3D printed actuator with an arbitrary pattern was developed and characterized based on different sizes, electrolyte concentration, input magnitudes, and frequencies. Then, a linear transfer function of the 3D printed polyelectrolyte soft actuator was developed to estimate the actuator behavior at different voltage signals. T-S fuzzy model was further employed for better presentation of actuator model in a range of voltage variations via interrelating the voltage dependent models. The experimental results showed improved performance obtained by using T-S fuzzy model compared to linear transfer function at different voltages. The proposed model could be used for other 3D printed soft actuators with custom design geometries due to its scalability.

References

1. A. Zolfagharian, A.Z. Kouzani, S.Y. Khoo, A.A.A. Moghadam, I. Gibson, A. Kaynak: Sens. Actuators, A Vol. 250 (2016), p. 258-272.
2. J. Ma, B. Franco, G. Tapia, K. Karayagiz, L. Johnson, J. Liu, R. Arroyave, I. Karaman, A. Elwany: Sci. Rep. Vol. 7 (2017), p. 46707.
3. A. Zolfagharian, A.Z. Kouzani, S.Y. Khoo, I. Gibson, A. Kaynak: *3D printed hydrogel soft actuators*, (IEEE, Singapore 2016).

4. A. Zolfagharian, A.Z. Kouzani, S.Y. Khoo, B. Nasri-Nasrabadi, A. Kaynak: Sens. Actuators, A Vol. 265 (2017), p. 94-101.
5. A. Zolfagharian, A. Kaynak, S.Y. Khoo, A.Z. Kouzani: 3D Printing and Additive Manufacturing, Vol. 5 (2018).
6. L. Elviri, R. Foresti, C. Bergonzi, F. Zimetti, C. Marchi, A. Bianchera, F. Bernini, M. Silvestri, R. Bettini: Biomed. Mater. Vol. 12 (2017), p. 045009.
7. T. Shiga, T. Kurauchi: J. Appl. Polym. Sci. Vol. 39 (1990), p. 2305-2320.
8. Y. Li, Y. Sun, Y. Xiao, G. Gao, S. Liu, J. Zhang, J. Fu: ACS Appl. Mater. Interfaces Vol. 8 (2016), p. 26326-26331.
9. J. Shang, Z. Shao, X. Chen: Biomacromolecules Vol. 9 (2008), p. 1208-1213.
10. V. Vunder, A. Punning, A. Aabloo, in: Ionic Polymer Metal Composites (IPMCs), edited by M. Shahinpoor RCS Publishing, 2015.
11. A. Attaran, J. Brummund, T. Wallmersperger: Smart Mater. Struct. Vol. 24 (2015), p. 035021.
12. Y. Bar-Cohen: Electroactive polymer (EAP) actuators as artificial muscles: reality, potential, and challenges (SPIE press, 2004).
13. Y. Liu, R. Zhao, M. Ghaffari, J. Lin, S. Liu, H. Cebeci, R.G. de Villoria, R. Montazami, D. Wang, B.L. Wardle: Sens. Actuators, A Vol. 181 (2012), p. 70-76.
14. T. Takagi, M. Sugeno: Elsevier (1993), p. 387-403.
15. S. Nasiri, M.R. Khosravani, K. Weinberg: Eng. Fail. Anal. Vol. 81 (2017), p. 270-293.
16. A. Zolfagharian, A.Z. Kouzani, S.Y. Khoo, A. Noshadi, A. Kaynak: Smart Mater. Struct. 27 (2018), p. 045019.
17. P.G.A. Madden, Massachusetts Institute of Technology, (2003).
18. S. Nemat-Nasser, J.Y. Li: J. Appl. Phys. Vol. 87 (2000), p. 3321-3331.
19. Y. Fang, X. Tan, Y. Shen, N. Xi, G. Alici: Mater. Sci. Eng. C, Vol. 28 (2008), p. 421-428.
20. X. Yu, Z. Man, B. Wu: Fuzzy Sets Syst. Vol. 95 (1998), p. 295-306.
21. B. Golubev, I. Horowitz: Int. J. Control Vol. 82, p. 711-723.
22. A. Noshadi, A. Zolfagharian, G. Wang: Trans Tech Pub Vol. 110 (2012), p. 4932-4940.
23. A. Zolfagharian, A. Z. kouzani, A. A. A. Moghadam, S. Y. Khoo, S. Nahavandi, A Kaynak: Smart Mater. Struct. (2018).
24. I. Benedetti, H. Nguyen, R. A. Soler-Crespo, W. Gao, L. Mao, A. Ghasemi, , J. Wen, S. Nguyen, H. D. Espinosa: J. Mech. Phys. Solids, Vol. 112 (2018), p. 66-88.
25. P. C. Innis, J. Chen, W. Zheng: Mechanism in charge transfer and electrical stability. In Conductive Polymers (CRC Press, 2017).

© 2018 by the authors. Submitted for possible open access publication under the terms and conditions of the Creative Commons Attribution (CC BY) license (http://creativecommons.org/licenses/by/4.0/).